







Broadband infrared and THz transmitting silicon core optical fiber

TRYGVE SØRGÅRD,¹  SEUNGHAN SONG,¹ PER ERIK VULLUM,^{1,2}
CRISTINE KORES,³  KJELL MARTIN MØLSTER,³ FREDRIK
LAURELL,³ THOMAS HAWKINS,⁴ JOHN BALLATO,⁴  ULF L.
ÖSTERBERG,^{3,5} AND URSULA J. GIBSON^{1,3,*} 

¹Department of Physics, Norwegian University of Science and Technology, Trondheim NO-7491, Norway

²SINTEF Industry, NO-7046, Trondheim, Norway

³Department of Applied Physics, Royal Institute of Technology, KTH, 10691 Stockholm, Sweden

⁴Department of Materials Science and Engineering, Clemson University, Clemson SC 29634, USA

⁵Thayer School of Engineering, Dartmouth College, Hanover NH 03755, USA

*ursula.gibson@ntnu.no

Abstract: Silicon waveguide structures are a viable alternative for the transmission of signals over a wide range of frequencies, and new fabrication methods are key to increased applications. In this work, THz transparency of silicon-core, silica clad fibers, refined using a traveling solvent method, is demonstrated. The $\approx 200\ \mu\text{m}$ core of these fibers is shown to have good transmission from 4.8–9 μm and 1–7 THz. Fibers were drawn on a conventional optical fiber tower using the scalable molten core technique and CO₂ laser annealed, resulting in large-grain crystalline cores with broadband transmission. The spectral properties are comparable to those of rectangular guides of similar cross-sectional area cut from high resistivity float zone silicon wafers.

© 2020 Optical Society of America under the terms of the [OSA Open Access Publishing Agreement](#)

1. Introduction

The infrared (IR) and terahertz (THz) regions of the electromagnetic spectrum are finding increasing utility for medical diagnosis due to the spectral signatures of biomolecules [1], and THz frequencies are being explored as a supplement to crowded telecommunications bands [2]. Due to strong absorption of THz wavelengths by humid air, proposed applications in this band require the development of low loss waveguides, and many approaches have been assessed. THz radiation, in particular is challenging because the free-space wavelengths are on the order of 300 μm , making waveguide propagation difficult, even with large index of refraction materials, for core dimensions less than 40 μm . Microfabrication has been used extensively for integrated devices [3,4], and hollow metal tubes have been used as waveguides up to ~ 2 THz [5]. Photonic crystal fibers have also been studied, and flexible Teflon guides of up to 15 cm in length with losses of 0.1 to 0.2 cm^{-1} below 1 THz have been reported, but with thicknesses of ~ 5 mm [6]. Ribbon-type guides [7] based on polymer-clad high index material have been investigated, but still have predicted losses an order of magnitude higher than a high resistivity silicon ribbon, and require dry air for good transmission. Malekabadi [8] gives an excellent review of solid core structures, and presents results in the microwave region, discussing the superiority of high purity silicon; it is seen as the best broad transmission window option [7]. Silicon core fibers have been analyzed as potential waveguides [9], and recent experimental studies on planar guides support the validity of this approach [10]. A major challenge for fibers is the preference for a single or near-single crystal core to limit impurity inclusion and scattering losses but most studies on the recrystallization of silicon fibers have been done with smaller core material [11–13]. Recent advances in laser treatment have used an alloying element [14,15] to promote formation of single crystal large-core materials. Here, we report on broadband THz and infrared (IR) transmission of

silicon-core samples fabricated using eutectic alloy annealing on molten-core drawn fibers, and compare them to rectangular guides made from high resistivity float-zone (HRFZ) silicon wafers.

2. Experimental

Rectangular guides were made from a 300 μm thick HRFZ ($\rho > 20,000$ ohm-cm) Si wafer (El-Cat) diced with nominal 250 μm spacing using a precision saw (DISCO DAD-2H6M). Subsequently, the samples were rotated by 90°, and another dicing step was carried out to decrease the height of the guides to 110–120 μm . The resultant slivers were either placed in glass capillaries to simplify handling in the FTIR, or mounted between two fused silica flats, with IR and THz absorbing wax filling any gaps. The end faces of samples were hand-polished using a series of abrasive papers with grits from 15 to 1 μm , but sides were as-cut. Silica clad optical fibers were drawn using the molten core method, [16] with a mixed core of HRFZ ($\rho > 5,000$ ohm-cm) silicon and 10 at% Au. Eutectic systems allow laser-driven directional solidification of well-ordered crystalline samples for large core diameters, as seen by Song, et al. [14]. Directional recrystallization and removal of the gold from the 210 ± 5 μm diameter, 0.035 mm^2 core was performed using a CO₂ laser-based commercial tapering system (NYFORS SMARTSPLICER). Treatment was performed using 4.5–5.5 W of power and a scan rate of 0.02 mm/s. The slow translation speed allowed effective removal of the gold, but the heavy gold loading in the original fiber limited the length over which the laser was able to transport the removed material. Multiple passes or lower gold concentrations could ameliorate this challenge. Gold was chosen for the relatively low eutectic temperature, low solid solubility in Si [17] and because it would not react with the silica during the drawing process, as observed with aluminum [18].

Sample dimensions were measured using a combination of X-ray computed tomography (XCT) and optical microscopy (Nikon SMZ1000). XCT data was taken with an XT H 225 ST micro-CT system from Nikon Metrology NV, using a source current of 47 μA and acceleration voltage of 145 kV and a tungsten target. Scanning electron microscope (SEM) micrographs were acquired using an FEI APREO operating at an accelerating voltage of 10 kV in back-scattered electron (BSE) analysis mode and an 80 mm^2 Oxford Xmax Energy dispersive X-ray spectrometer (EDS) was used for composition determinations.

To assess the crystalline and optical quality of the silicon core, X-ray diffraction (XRD), transmission electron microscopy (TEM) and Fourier transform infrared (FTIR) transmission measurements were made. X-ray characterization of the silicon core fiber was performed with a Bruker D8 Advance powder diffractometer using a 15 mm wide beam from a Mo $K\alpha_{1,2}$ X-ray source ($\lambda = 0.7093$ Å, 0.7139 Å). Fibers were mounted in the capillary holder, and the fiber axis was optically aligned perpendicular to the X-ray scattering plane. After alignment, conventional $\theta - 2\theta$ scans were taken with a θ step of 0.01° and a full rotation of the fiber at each step. In addition to conventional scans, for each observed Bragg reflection, X-ray intensity was recorded as a function of the fiber's axial rotational position (ϕ scan). This allowed analysis of the number and orientation of crystal grains within the core [14]. The rectangular guides were cut from single crystal wafers and thus no XRD was performed. The plane-view TEM sample was prepared by focused ion beam (FIB), using a Helios G4 UX from FEI. Coarse thinning was performed at 30 kV ion beam acceleration voltage. Final thinning was performed first at 5 kV and then 2 kV on either side of the TEM lamella to minimize ion beam induced surface damage. TEM studies were performed with a double Cs aberration corrected cold FEG JEOL ARM 200CF, operated at 200 kV.

Infrared transmission scans were made from 2.5–25 μm in a Bruker 27 FTIR with a 6x beam condenser from Pike Technologies. IR opaque material was used to mount the waveguides in the sample holder to eliminate stray light. A rectangular HRFZ waveguide (area ~ 0.03 mm^2 , length 8.4 mm) for FTIR measurements was mounted in IR opaque, low temperature melting wax (Ted

Pella) inside a borosilicate capillary, and polished to expose the waveguide ends. The wax had an IR cutoff of about $2.7\ \mu\text{m}$, assuring that any long wavelength signal came through the silicon.

Terahertz transmission measurements were made with the broadband plasma-based system described in [10], but with the sample placed between the off-axis parabolic mirrors, as shown in Fig. 1. The system geometry limited the sample lengths to a maximum of 18 mm. The sample was mounted in a metal aperture in order to minimize THz radiation leakage around the sample edges. The arrival time of the THz signal could be used to distinguish between any silica cladding transmission and the signal through the silicon core. The output lens position was kept constant, and for the reference measurement the input lens was moved so that the lenses were confocal. The separation between the lenses and the input and output faces of the guide could be adjusted to give optimal coupling, and the fiber could be translated laterally relative to the axis of the THz beam for alignment purposes. The probe pulse, with arrival time controlled by a motorized delay stage, passed through a hole in the second parabolic mirror to allow co-propagation with the THz beam, and a $300\ \mu\text{m}$ thick gallium phosphide (GaP) crystal was used for electro-optic detection.

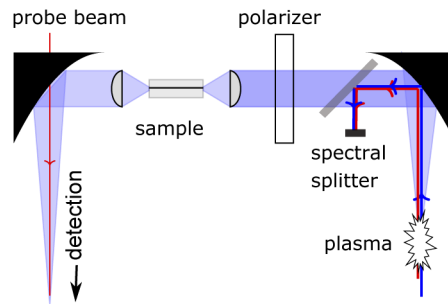


Fig. 1. THz experimental setup for waveguide transmission measurements.

3. Results and discussion

X-ray diffraction analysis indicated that the Si-core fiber was highly crystalline after the Au-assisted laser treatment. A $15\ \text{mm}$ wide beam and conventional $\theta - 2\theta$ scan, as shown in Fig. 2(a), indicated no residual metallic gold on the micron scale; this was confirmed with x-ray imaging. Additional x-ray scans taken with a reduced beam size at different positions along the fiber allowed resolution of two Si grains along the axis, identified by the red and blue tags in the figure. The larger of these two grains was oriented with a $\langle 110 \rangle$ direction along the axis. The inset shows the location of the grain boundary, approximately $3\ \text{mm}$ from one end of the fiber. Figure 2(b) presents axial (ϕ) rotational scans from $0-180^\circ$ for the $\{004\}$, $\{111\}$ and $\{220\}$ Bragg peaks of the 'red' grain, where the angular separation of the peaks indicates the crystal symmetries and orientation [14] (scans from $180-360^\circ$ were identical). Such simple grain structure is not seen in the as-drawn fibers, and has not been observed previously for pure silicon fibers with such large core diameters; the gold permits traveling solvent recrystallization [19] with the silica cladding acting as a crucible. Figure 2(c) shows electron diffraction from a FIB-extracted slice parallel to the face of the core, indicating the silicon to be of high quality on the nanoscale and confirming the core axial orientation.

Figure 3(a)-(d) show additional structural analysis of the fiber core. EDS indicates oxygen levels less than 1.5% and a gold signal that is in the noise. Contributions to the oxygen signal may be from oxidation of the Si surface or stray radiation from the SiO_2 surrounding the Si core. TEM analysis on the core revealed a small number of dislocations and twins, some of which were decorated by gold nanoparticles, as shown in Fig. 3(e) and (f).

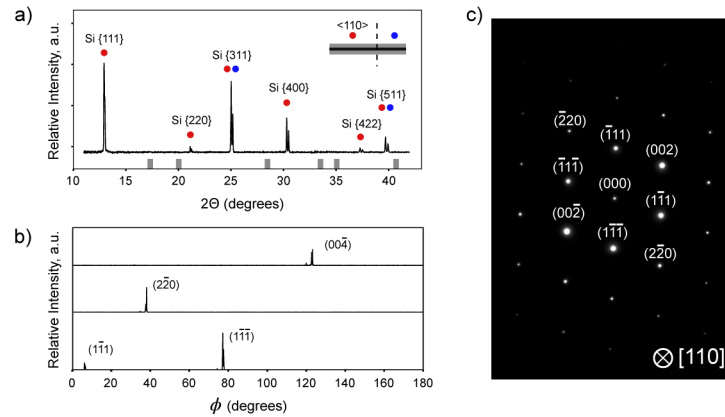


Fig. 2. Diffraction patterns of the 9.6 mm long silicon core fiber made by removal of Au. (a) Bragg reflections of rotating fiber; red and blue tags indicate from which part of the fiber (as shown in the inset) peaks originate. Gray ticks on the x-axis indicate gold Bragg angles. (b) ϕ scans for {004}, {220} and {111} reflections. (c) electron diffraction from thin section of core material.

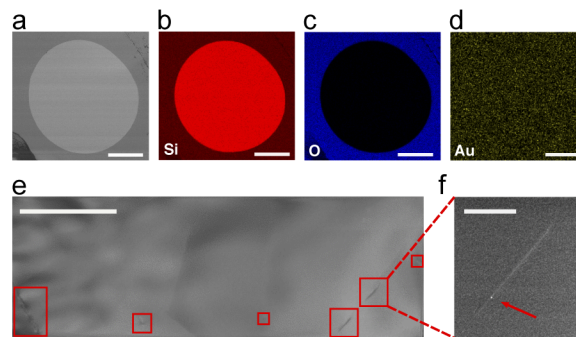


Fig. 3. SEM and TEM characterization of the core (a) BSE image, (b) silicon EDS map, (c) oxygen EDS map, (d) gold EDS map. Scale bars 60 μm . (e) A bright field (BF) TEM image showing defects in the silicon (scale bar 2 μm), and (f) a gold nanoparticle decorating a dislocation found in a high angle annular dark field (HAADF) STEM image (scale bar 200 nm).

FTIR transmission results from 4–12 μm for a silica-only fiber, a silicon core (silica-clad) fiber from which gold had been removed, and a rectangular silicon waveguide are presented in Fig. 4. Averages of several runs with different alignment are presented, as the absolute magnitudes of the signals varied due to alignment and the small waveguide dimensions. Spectral features were reproducible. The silica-only fiber (9 mm long, 0.8 mm^2 area) showed no transmission beyond 5 μm , while the transmission through the 9.6 mm long Si/silica fiber (core area $\sim 0.035 \text{ mm}^2$) extended to 10 μm . Transmission of wavelengths $<4 \mu\text{m}$ through the cladding was $\sim 4\%$ while that of IR through the core was $\sim 0.18\%$, scaling with the cladding vs. core area (20x) and the reflection losses expected for the silica and silicon materials. Comparable signal strengths through the fiber and the 8.4 mm rectangular guide (0.03 mm^2 area) suggest slightly higher losses ($\sim 10\%$) in the gold-treated material, but transmission values had large uncertainties, as indicated by the signal strength range bar in Fig. 4. Features in the silicon-core IR fiber spectrum are similar to those seen in commercially available uncoated silicon windows. Phonon absorption in silicon results in several absorption bands in the region 7–16 μm [20], and oxygen incorporation

(e.g. as observed in Czochralski growth) is responsible for strong extinction at $9.2\ \mu\text{m}$ [21]. Gold acceptor and donor levels in silicon lie respectively 0.55 and 0.61 eV from the band edges [22], measured by photoemission at 90 K. Those measurements gave an absorption threshold around 0.4 eV ($2.5\ \mu\text{m}$), which would be broadened at room temperature, but silica transmission obscures the core properties in this region.

Figure 5 shows THz time-domain spectroscopy (TDS) measurements of a 9.6 mm long fiber ($210\ \mu\text{m}$ core diameter) and a 13 mm long, $120 \times 290\ \mu\text{m}$ as-sawn rectangular waveguide. The x-axes show the delay time with respect to the reference pulse and are shifted to facilitate comparison of the pulse shapes. The small thickness of the GaP crystal caused Fabry-Pérot echoes [10] in the time-domain signal. Reflections inside the GaP crystal occur at intervals of ~ 6 ps, and are clearly observed in all three traces. The peak signals are of comparable magnitude, but the rectangular waveguide, which is longer than the silicon core fiber, shows a longer dispersed low frequency tail and a less regular waveform.

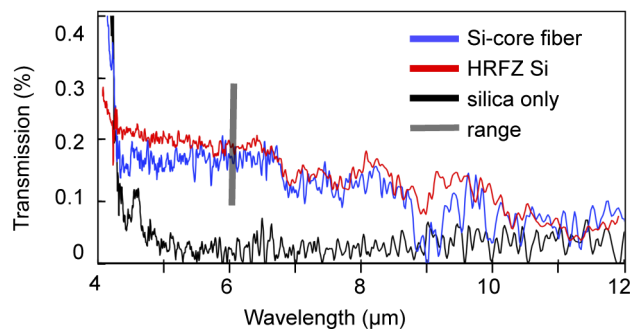


Fig. 4. FTIR spectra of silica fiber (black), silicon core fiber (blue), and rectangular HRFZ Si waveguide (red). Gray vertical bar indicates range of signal magnitudes.

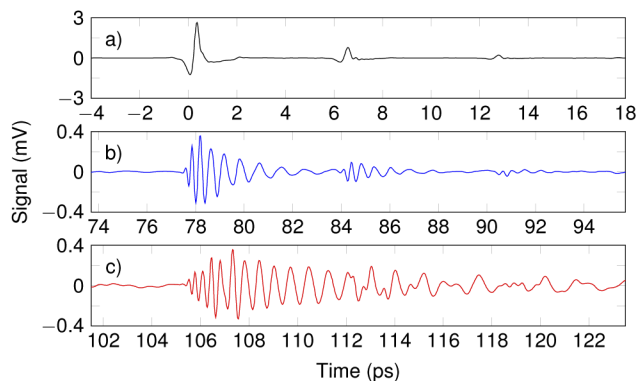


Fig. 5. Time traces of (a) the dry air reference when no sample is present (black), (b) a 9.6 mm long $210\ \mu\text{m}$ diameter core fiber (blue) and (c) a rectangular guide, (area $\sim 0.03\ \text{mm}^2$, length 13 mm) (red).

Figure 6 shows the Fourier transform of the signals from the two samples (inset: cross-sectional images). The small oscillations in the frequency spectra are due to the inclusion of the Fabry-Pérot echoes in the time-domain. The waveguide signal levels are comparable above ~ 2 THz, with the roll-off for the fiber at low frequencies being more pronounced. Based on the absorption curves for fused silica from [23], it is likely that the low-frequency roll-off of the spectrum is due, at least in part, to increased cladding interactions. Both the roll-off and dips in the rectangular

waveguide spectrum (e.g. at 3.5 and 5 THz) are sensitive to the exact coupling conditions (see [Appendix](#)). Signal reduction after transmission through either sample was less than 4 dB in the range 2–6 THz. Based on the cross sectional areas and lengths, comparable transmission values imply an average absorption coefficient difference of less than 10 % for the two materials in this range. The coupling is likely responsible for much of this loss, as the material absorption of the HRFZ Si is known to be low [24]. Coupling efficiency improvement may be possible using structures such as those described by Kim, et al. [25].

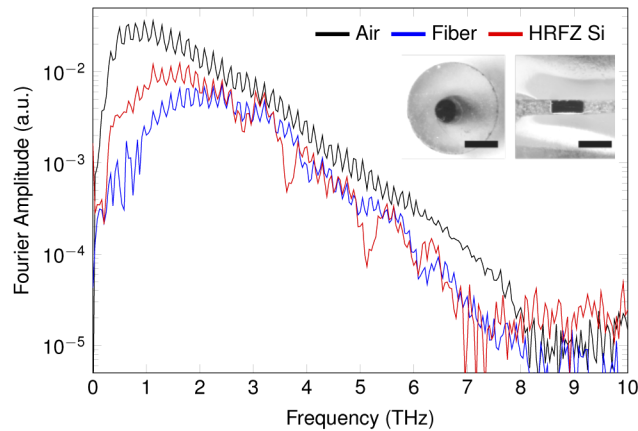


Fig. 6. Fourier transforms of THz signals for dry air reference (black), a 9.6 mm long silicon core fiber (blue) and a 13 mm long rectangular-cut HRFZ wafer (red). Scale bars on inset are 300 μm.

Figure 7 shows Wigner-Ville (W-V) representations of frequency/time signals for the fiber (panels (a) and (b)) and the rectangular waveguides (panels (c) and (d)), with displaced, but identical scale time axes. The W-V plot for the rectangular guide has a broad main peak that is believed to arise from coupling considerations, as the position and intensities of the associated transmission dips are a function of exact alignment. Measurements in the reference configuration but with a varying diameter aperture before the input lens demonstrated some radial dependence of the frequency content of the pulses, and the larger size of the rectangular guide in one dimension may have made coupling for this guide more sensitive to the input conditions.

The transmission properties observed here were only seen for laser-driven traveling solvent refined fibers. For this method, the choice of solvent should be made with the application of the fiber in mind; any residual atomic gold dissolved in the Si will form deep traps, increasing absorption of photons with energies above ~ 0.5 eV [22], but should not limit mid IR and THz transmission. Small numbers of nanoparticles (less than 10 nm diameter) did not significantly affect the transmission. Binary or tertiary semiconductor systems are another option, where the metal is replaced with elements that form alloy or pseudo-eutectic systems. Instead of introducing discrete levels, these elements may alter the bandgap of the material. SiGe is an illustrative example; under equilibrium conditions, it forms a homogeneous solid solution for all compositions. However, solidification kinetics are an important consideration; at sufficiently high cooling rates, diffusion-limited inhomogeneity can be used to drive the formation of useful compositional microstructures [26,27]. Recent work on radially varying semiconductor composition in SiGe fibers [28] is promising for reduction of cladding losses with smaller cores. The pseudo-eutectic systems such as GaSb in Si are another option, but may have high conductivity if residual unbonded Group III or V elements remain, reducing the transparency window.

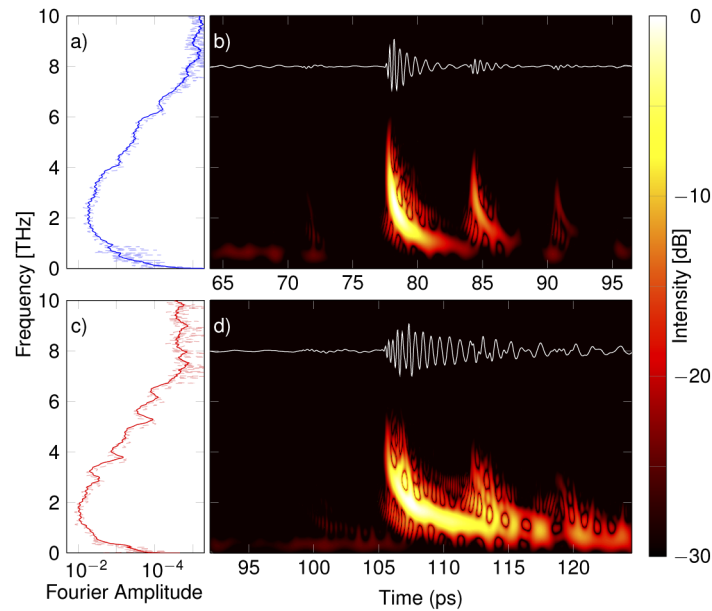


Fig. 7. (a) Frequency and (b) Wigner-Ville representation of fiber transmission signal and (c) frequency and (d) Wigner-Ville plots for a rectangular waveguide signal. Solid lines in frequency plots present moving averages over the GaP reflections. White lines in the Wigner-Ville figures show the measured THz time-domain spectroscopy signals.

4. Conclusion

The silicon core fiber made by molten core drawing, a scalable manufacturing method, showed transmission in both broad infrared- and THz bands - comparable to HRFZ samples despite a low density of nanometer-size gold inclusions. This opens up the possibility of using the molten core fiber technique for fabrication of waveguides and biocompatible THz probes; other demonstrated waveguides are either larger or suffer from significant bending losses. Although this first demonstration of guiding in fibers used short, large diameter samples, a fiber tip of this material could be combined with a longer guide lacking biocompatibility. Results on wafers [10] demonstrate that smaller diameters where fiber flexibility is maintained could also be developed.

The traveling solvent method of material refinement, adapted to the fiber geometry, led to a large diameter core with a single grain boundary. For long wavelength applications, it is shown that a eutectic-forming metal associated with deep trap levels is a suitable solvent.

Appendix

Figure 8 shows an additional measurement of the rectangular sample, where the frequency spectrum lack sharp dips, verifying that those features are coupling-dependent. This measurement had a different baseline than the other data, and was therefore not incorporated into Fig. 6 of the main article, as signal magnitudes are not directly comparable.

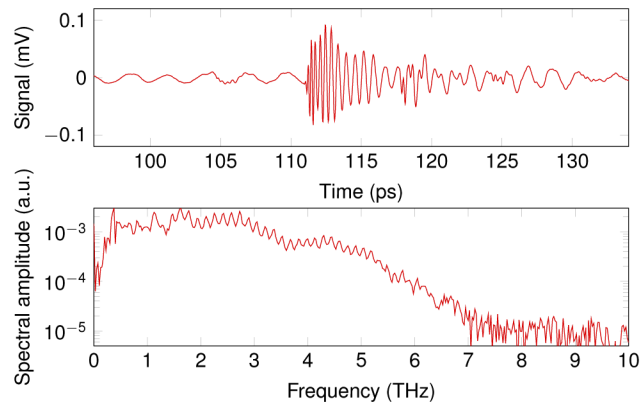


Fig. 8. Time-domain signal (top) and Fourier transform (bottom), of the rectangular guide after removal from and reinsertion into the THz sample holder.

Funding

Norges Forskningsråd (262232, 262644); NORTEM (197405); NoRFab (245963/F50); Norges Teknisk-Naturvitenskapelige Universitet; Knut och Alice Wallenbergs Stiftelse (2016.0104); Vetenskapsrådet (2016-04488); J. E Sirrinc Foundation.

Disclosures

The authors declare no conflicts of interest.

References

1. L. Yu, L. Hao, T. Meiqiong, H. Jiaoqi, L. Wei, D. Jinying, C. Xueping, F. Weiling, and Z. Yang, "The medical application of terahertz technology in non-invasive detection of cells and tissues: opportunities and challenges," *RSC Adv.* **9**(17), 9354–9363 (2019).
2. Z. Chen, X. Ma, B. Zhang, Y. Zhang, Z. Niu, N. Kuang, W. Chen, L. Li, and S. Li, "A survey on terahertz communications," *China Commun.* **16**(9), 1–14 (2019).
3. K. Tsuruda, M. Fujita, and T. Nagatsuma, "Extremely low-loss terahertz waveguide based on silicon photonic-crystal slab," *Opt. Express* **23**(25), 31977–31990 (2015).
4. H. Amarloo and S. Safavi-Naeini, "Terahertz line defect waveguide based on silicon-on-glass technology," *IEEE Trans. Terahertz Sci. Technol.* **7**(4), 433–439 (2017).
5. G. Gallot, S. P. Jamison, R. W. McGowan, and D. Grischkowsky, "Terahertz waveguides," *J. Opt. Soc. Am. B* **17**(5), 851–863 (2000).
6. M. Goto, A. Quema, H. Takahashi, S. Ono, and N. Sarukura, "Teflon photonic crystal fiber as terahertz waveguide," *Jpn. J. Appl. Phys.* **43**(No. 2B), L317–L319 (2004).
7. C. Yeh, F. Shimabukuro, and P. H. Siegel, "Low-loss terahertz ribbon waveguides," *Appl. Opt.* **44**(28), 5937–5946 (2005).
8. A. Malekabadi, S. A. Charlebois, D. Deslandes, and F. Boone, "High-resistivity silicon dielectric ribbon waveguide for single-mode low-loss propagation at F/G-bands," *IEEE Trans. Terahertz Sci. Technol.* **4**(4), 447–453 (2014).
9. D. A. Bas, S. K. Cushing, J. Ballato, and A. D. Bristow, "Terahertz waveguiding in silicon-core fibers," arXiv:1305.0520 (2013).
10. T. Sjørgård, K. M. Mølster, F. Laurell, V. Pasiskevicius, U. J. Gibson, and U. L. Österberg, "Terahertz waveguiding in glass-clad silicon wafers," *Opt. Mater. Express* **10**(3), 742–751 (2020).

11. N. Healy, M. Fokine, Y. Franz, T. Hawkins, M. Jones, J. Ballato, A. C. Peacock, and U. J. Gibson, "CO₂ laser-induced directional recrystallization to produce single crystal silicon-core optical fibers with low loss," *Adv. Opt. Mater.* **4**(7), 1004–1008 (2016).
12. Y. Franz, A. F. J. Runge, H. Ren, N. Healy, K. Ignatyev, M. Jones, T. Hawkins, J. Ballato, U. J. Gibson, and A. C. Peacock, "Material properties of tapered crystalline silicon core fibers," *Opt. Mater. Express* **7**(6), 2055–2061 (2017).
13. Z. Zhao, L. Ren, J. Zhang, S. Wang, F. Xue, and Y. Mao, "High temperature annealing of si core fiber with different annealing time," *Opt. Fiber Technol.* **58**, 102288 (2020).
14. S. Song, K. Lønsethagen, F. Laurell, T. W. Hawkins, J. Ballato, M. Fokine, and U. J. Gibson, "Laser restructuring and photoluminescence of glass-clad GaSb/Si-core optical fibres," *Nat. Commun.* **10**(1), 1790 (2019).
15. W. Wei, S. Song, M. H. Balci, F. Laurell, P. R. Cantwell, J. Ballato, and U. J. Gibson, "Single crystal semiconductor-core optical fiber," in *Sixth Intl WSOF 2019*, vol. 11206; J. Ballato and L. Dong, eds. (SPIE, 2019), pp. 1120615:1–4.
16. J. Ballato and A. C. Peacock, "Perspective: Molten core optical fiber fabrication route to new materials and applications," *APL Photonics* **3**(12), 120903 (2018).
17. M. Brown, C. L. Jones, and A. F. Willoughby, "Solubility of gold in p-type silicon," *Solid-State Electron.* **18**(9), 763–770 (1975).
18. C. Hou, X. Jia, L. Wei, S.-C. Tan, X. Zhao, J. D. Joannopoulos, and Y. Fink, "Crystalline silicon core fibres from aluminium core preforms," *Nat. Commun.* **6**(1), 6248 (2015).
19. G. A. Wolff and A. I. Mlavsky, "Travelling solvent techniques," in *Crystal Growth: Theory and Techniques Volume 1*, C. H. L. Goodman, ed. (Springer US, 1974), pp. 193–232.
20. M. Pradhan, R. Garg, and M. Arora, "Multiphonon infrared absorption in silicon," *Infrared Phys.* **27**(1), 25–30 (1987).
21. C. R. Poznich and J. C. Richter, "Silicon for use as a transmissive material in the far IR," in *Window and Dome Technologies and Materials III*, vol. 1760 P. Klocek, ed., International Society for Optics and Photonics (SPIE, 1992), pp. 112–120.
22. S. Braun and H. G. Grimmeiss, "Optical properties of gold acceptor and donor levels in silicon," *J. Appl. Phys.* **45**(6), 2658–2665 (1974).
23. M. Naftaly and R. E. Miles, "Terahertz time-domain spectroscopy of silicate glasses and the relationship to material properties," *J. Appl. Phys.* **102**(4), 043517 (2007).
24. K. Mølster, "THz time domain spectroscopy of materials in reflection and transmission," Master's thesis, Department of Electronic Systems, Faculty of Information Technology and Electrical Engineering, NTNU (2017).
25. S.-H. Kim, E. S. Lee, Y. B. Ji, and T.-I. Jeon, "Improvement of THz coupling using a tapered parallel-plate waveguide," *Opt. Express* **18**(2), 1289–1295 (2010).
26. D. A. Coucheron, M. Fokine, N. Patil, D. W. Breiby, O. T. Buset, N. Healy, A. C. Peacock, T. Hawkins, M. Jones, J. Ballato, and U. J. Gibson, "Laser recrystallization and inscription of compositional microstructures in crystalline SiGe-core fibres," *Nat. Commun.* **7**(1), 13265 (2016).
27. W. Wu, M. H. Balci, K. Mühlberger, M. Fokine, F. Laurell, T. Hawkins, J. Ballato, and U. J. Gibson, "Ge-capped SiGe core optical fibers," *Opt. Mater. Express* **9**(11), 4301–4306 (2019).
28. W. Wu, M. Balci, S. Song, C. Liu, M. Fokine, F. Laurell, T. Hawkins, J. Ballato, and U. J. Gibson, "CO₂ laser annealed SiGe core optical fibers with radial Ge concentration gradients," *Opt. Mater. Express* **10**(4), 926–936 (2020).